

Lepton flavor violation in muonium decay and muon colliders in models with heavy neutrinos

G. Cvetič* and C. Dib†

Dept. of Physics, Universidad Técnica Federico Santa María, Valparaíso, Chile

C. S. Kim‡

Department of Physics, Yonsei University, Seoul 120-749, Korea

J. D. Kim§

Department of Physics, Seoul National University, Seoul 151-742, Korea

We study the lepton-flavor-violating reaction $\mu^+e^- \rightarrow e^+e^-$ within two extensions of the standard model that include heavy neutrinos. The reaction is studied in the low energy limit in the form of muonium decay $M \rightarrow e^+e^-$ and in the high energy regime of a muon collider. The two theoretical models we consider are: model I, a typical see-saw model that violates lepton flavor and number by inclusion of extra right handed neutrinos, and model II, a variant where lepton number is conserved and which includes extra right handed as well as left handed neutrinos, singlets under the gauge group. We find for muonium decay into e^+e^- the extremely small result $Br(M \rightarrow e^+e^-) < 10^{-19}$ in both scenarios. Alternatively, for μ^+e^- collisions up to $\sqrt{s} \sim 50$ GeV we find $\sigma(\mu^+e^- \rightarrow e^+e^-) < 10^{-5}$ fb, while for energies above the W^+W^- threshold we find $\sigma(\mu^+e^- \rightarrow W^+W^-)$ up to ~ 1 fb.

PACS numbers: 14.60.St, 14.60.Ef, 14.60.Pq, 13.66.Lm, 25.30.Mr

I. INTRODUCTION

A current issue in particle physics is the understanding of the neutrino sector. It is by now consistent with experimental results to assert that at least some of the standard neutrinos must have small (but non-zero) masses and these mass states should mix under the weak interactions[1]. As a consequence, the lightness of the standard neutrinos ($m_\nu \lesssim 1$ eV) compared to the charged leptons (\gtrsim MeV) remains to be understood. If neutrinos are of a Dirac nature, non-zero masses can appear in the standard model (SM) by inclusion of (sterile) right-handed neutrinos[2]. If neutrinos are of a Majorana nature –a more general case–, more appealing solutions exist in the context of extended gauge structures. An interesting solution is provided by the so-called seesaw mechanism within $SO(10)$ or left-right symmetric models of interactions. In conventional seesaw models, the effective light neutrino masses are within the scales of eV to MeV via a relation involving the hierarchy between very large Majorana masses and Dirac masses comparable to those of the charged leptons[3]. Another possible solution was investigated in the framework of heterotic superstring models [4] with E_6 symmetry or certain scenarios of $SO(10)$ models [5], where the low-energy effective theories include new left-handed and right-handed neutral isosinglets and assume conservation of total lepton number in the Yukawa sector.

One avenue to study the neutrino sector is to consider lepton flavor violating processes (LFV) of standard particles, which are absent in the SM and depend on neutrino masses and mixings. Free lepton decays like $\mu \rightarrow e\gamma$, $\mu \rightarrow 3e$, $\tau \rightarrow 3\mu$, etc. are among the most direct LFV processes and they have been studied in detail [6]-[11],[15]. Other ways like muon-to-electron conversion in nuclei and muonium-to-antimuonium conversion are also possibilities [12, 13, 16]. Yet another possibility is to consider lepton-lepton scattering or bound state decays (e.g. muonium decay). These modes contain the same underlying physics as free lepton decays, but differ in the experimental conditions and, from the phenomenological viewpoint they are sensitive to other combination of parameters because of their different kinematical regime.

*Electronic address: gorazd.cvetic@usm.cl

†Electronic address: claudio.dib@usm.cl

‡Electronic address: cskim@yonsei.ac.kr

§Electronic address: jade@phy.snu.ac.kr

In this work we study the process $\mu^+e^- \rightarrow e^+e^-$ at low energy in the form of muonium decay (muonium is a non-relativistic μ^+e^- bound state) and at high energy in the form of μ^+e^- collisions. Muonium is formed when a μ^+ slows down inside a material and captures an electron, forming a bound state due to Coulomb attraction. The fraction of muons that actually end up as muonium depends very much on the material, ranging from small fractions in some to nearly 100% in others. Most muonia decay as $M \rightarrow e^+e^-\bar{\nu}_\mu\nu_e$, which is simply a muon decay with an electron as spectator [14]. A more rare mode, albeit standard, is annihilation $M \rightarrow \bar{\nu}_\mu\nu_e$, whose rate is $\sim 10^{-11}$ times smaller. Here we study the mode $M \rightarrow e^+e^-$, which violates lepton flavor and is thus forbidden in the SM. From our point of view, muonium decay is interesting because it is a non-relativistic μ^+e^- process, and thus depends on different combinations of parameters than in high energy processes. Complementary to it, we also study the collision $\mu^+e^- \rightarrow e^+e^-$ at high energy. This process clearly requires a muon collider. We will not be exhaustive in the study of new physics at muon colliders but focus on this particular channel within the LFV models previously mentioned. In section II we give a brief review of the seesaw type models in question; in section III we describe the generic amplitudes for $\mu^+e^- \rightarrow e^+e^-$ processes within these models; section IV contains the application to muonium decay, section V the application to high energy collisions and section VI summarizes the results and conclusions.

II. TWO MODELS FOR HEAVY NEUTRINOS

Here we will briefly summarize the two models under consideration. Further details were given in previous works [15, 16]. The main features of these models are (i) they contain heavy neutrinos, (ii) in the mass eigenstate basis, the heavy neutrinos couple with charged leptons of mixed flavor under weak interactions (just like Cabbibo-Kobayashi-Maskawa mixing in the quark sector), and (iii) the neutrinos are generally of Majorana type.

Model I: This is a usual seesaw model [3]: it is the standard model with N_L generations (*i.e.* left-handed neutrinos ν_{iL}) and an equal number $N_H = N_L$ of right-handed neutrinos $\tilde{\nu}_{iR}$, singlets under the gauge group. The neutrino mass terms, after gauge symmetry breaking, are:

$$-\mathcal{L}_{\text{mass}}^\nu = \frac{1}{2} \left(\bar{\nu}_L, \bar{\nu}_R^c \right) \mathcal{M} \begin{pmatrix} \nu_L^c \\ \tilde{\nu}_R \end{pmatrix} + \text{h.c.} \quad (1)$$

The superscript c at some of the fields denotes charge-conjugated fields $\psi^c = \mathcal{C}\bar{\psi}^T$, where $\mathcal{C} = -i\gamma^2\gamma^0$ in the Dirac representation. The $2N_L \times 2N_L$ -dimensional matrix \mathcal{M} has a seesaw block form:

$$\mathcal{M} = \begin{pmatrix} 0 & m_D \\ m_D^T & m_M \end{pmatrix}, \quad m_D = \begin{pmatrix} a & b e^{i\delta_1} \\ c e^{i\delta_2} & d \end{pmatrix}, \quad m_M = \begin{pmatrix} M_1 & 0 \\ 0 & M_2 \end{pmatrix}, \quad (2)$$

The (real) parameters a, b, c, d in the Dirac mass matrix m_D are smaller than the Majorana mass parameters M_1 and M_2 ($M_2 \geq M_1 \gtrsim 100$ GeV) by at least an order of magnitude.

The squared ratio between the Dirac mass (m_D) and the Majorana mass (m_M) scales gives the order of magnitude of the heavy-to-light neutrino mixings $(s_L^\nu)^2 \equiv \sum_h |U_{hL}|^2 \sim |m_D|^2/|m_M|^2$. The physical light neutrino masses are of the order of $m_{\nu_{\text{light}}} \sim m_D^2/m_M$. The very low experimental bounds $m_{\nu_{\text{light}}} \lesssim 1$ eV impose in Model I severe constraints on the $|m_D| \ll |m_M|$ hierarchy required. The present experimental bounds on the heavy-to-light mixing parameters $(s_L^\nu)^2 \sim |m_D|^2/|m_M|^2$ ($\lesssim 10^{-2}$, see below) present another set of constraints on the model.

Model II: This model contains an equal number N_L of left-handed (S_{iL}) and right-handed ($\tilde{\nu}_{iR}$) neutral singlets [4, 5]. Furthermore, the form of the mass matrix \mathcal{M} leads to the conservation of total Lepton Number, although lepton flavor mixing is still possible. The neutrino mass terms, after electroweak symmetry breaking, have the form

$$-\mathcal{L}_{\text{mass}}^\nu = \frac{1}{2} \left(\bar{\nu}_L, \bar{\nu}_R^c, \bar{S}_L \right) \mathcal{M} \begin{pmatrix} \nu_L^c \\ \tilde{\nu}_R \\ S_L^c \end{pmatrix} + \text{h.c.}, \quad \mathcal{M} = \begin{pmatrix} 0 & m_D & 0 \\ m_D^T & 0 & m_M^T \\ 0 & m_M & 0 \end{pmatrix}, \quad (3)$$

and m_D and m_M are given in Eq. (2). The mass matrix \mathcal{M} is $(N_L + N_H) \times (N_L + N_H)$ -dimensional, $N_H = 2N_L$ (the Dirac block m_D is $N_L \times N_L$ -dimensional). The model, in its unperturbed form, predicts for each of the N_L generations a massless Weyl neutrino and two degenerate Majorana neutrinos [17, 18] ($N_H = 2N_L$). Therefore, the seesaw-type restriction $m_{\nu_{\text{light}}} \sim m_D^2/m_M$ of Model I is not present in Model II in its unperturbed form. However, present experimental bounds on heavy-to-light mixing parameters $(s_L^\nu)^2 \sim |m_D|^2/|m_M|^2$ ($\lesssim 10^{-2}$) do impose a certain level of hierarchy $|m_D| < |m_M|$ between the Dirac and Majorana mass sector, but is in general significantly weaker than in Model I. Nonzero masses of the N_L light neutrinos can be generated in Model II by introducing small

perturbations in the lower right block of \mathcal{M} , i.e., small Majorana mass terms for the neutral singlets S_{iL} , and this does not significantly affect the mixings of heavy-to-light neutrinos.

In either model, the mass matrix \mathcal{M} can always be diagonalized by means of a congruent transformation involving a unitary matrix U

$$UMU^T\Lambda^* = \mathcal{M}_d, \quad (4)$$

where $\mathcal{M}_d = \text{diag}(m_1, m_2, \dots)$ is the nonnegative diagonal mass matrix, and Λ^* is an arbitrary diagonal unitary matrix: $(\Lambda^*)_{ij} = \delta_{ij}\lambda_i^*$ and $|\lambda_i| = 1$. The $N_L + N_H$ mass eigenstates n_i are Majorana neutrinos, and are related to the interaction eigenstates ν_{kL} and $\tilde{\nu}_{jR}$ by the matrices U and Λ^* as:

$$\begin{pmatrix} \nu_L \\ \tilde{\nu}_R^c \end{pmatrix}_a = \sum_{i=1}^{N_L+N_H} U_{ia}^* n_{iL} \Rightarrow \begin{pmatrix} \nu_L^c \\ \tilde{\nu}_R \end{pmatrix}_a = \sum_{i=1}^{N_L+N_H} U_{ia} \lambda_i^* n_{iR}, \quad (5)$$

The first N_L eigenstates n_i ($i = 1, \dots, N_L$) are the light partners of the standard charged leptons. The other N_H eigenstates are heavy. It can be checked from relations (5) that the relation $(n_{iL})^c = \lambda_i^* n_{iR}$ holds, and thus λ_i is recognized as the creation phase factor [19, 20] of the Majorana neutrino n_i .

In the mass basis, a $N_L \times (N_L + N_H)$ -dimensional mixing matrix B for charged current interactions, and a $(N_L + N_H) \times (N_L + N_H)$ -dimensional matrix C for neutral current interactions can be introduced:

$$B_{li} = U_{il}^*, \quad C_{ij} = \sum_{a=1}^{N_L} U_{ia} U_{ja}^*. \quad (6)$$

Accordingly, the leptonic weak interactions are (cf. [16, 21])

$$\mathcal{L}_{lnW}(x) = \left(-\frac{g_w}{\sqrt{2}}\right) W_\mu^-(x) \sum_{i=1}^{N_L} \sum_{j=1}^{N_L+N_H} B_{ij} \bar{l}_i(x) \gamma^\mu P_L n_j(x) + \text{h.c.}, \quad (7)$$

$$\mathcal{L}_{lnG}(x) = \left(-\frac{g_w}{\sqrt{2}M_W}\right) G^-(x) \sum_{i=1}^{N_L} \sum_{j=1}^{N_L+N_H} B_{ij} \bar{l}_i(x) (m_{li} P_L - m_j P_R) n_j(x) + \text{h.c.}, \quad (8)$$

$$\mathcal{L}_{nnZ}(x) = \left(-\frac{g_w}{4} \frac{M_Z}{M_W}\right) Z_\mu^0(x) \sum_{i,j=1}^{N_L+N_H} \bar{n}_i(x) \gamma^\mu (C_{ij} P_L - C_{ij}^* P_R) n_j(x) + \text{h.c.}, \quad (9)$$

$$\mathcal{L}_{nnG}(x) = \frac{ig_w}{4M_W} G^0(x) \sum_{i,j=1}^{N_L+N_H} \bar{n}_i(x) \{i(m_j - m_i) \text{Im} C_{ij} + \gamma_5(m_j + m_i) \text{Re} C_{ij}\} n_j(x), \quad (10)$$

where G^- and G^0 are the Goldstone bosons that appear in a general gauge. Here, the conventions of Itzykson and Zuber[22] are used; $P_L = (1 - \gamma_5)/2$, $P_R = (1 + \gamma_5)/2$; l_i is the i -th negatively charged lepton ($l_1 = e^-$, $l_2 = \mu^-$); g_w is the $SU(2)_L$ coupling constant ($g_w^2 = 8G_F M_W^2/\sqrt{2}$) and n_j are the Majorana neutrinos (mass eigenstates).

In all our numerical calculations we will just use two generations (i.e. $N_L = 2$), since a third generation does not make a sizable change in our results, considering the uncertainties involved.

III. TRANSITION AMPLITUDE FOR $\mu^+ e^- \rightarrow e^+ e^-$

The amplitude for this process is similar to those of Ref. [7] for lepton decays. Just as in that case, the amplitude for $\mu^+ e^- \rightarrow e^+ e^-$ can be calculated neglecting external momenta and external masses inside the loop, provided the neutrinos in the loop are heavy. Let us define the kinematics of the process as:

$$\mu^+(k_1) e^-(k_2) \rightarrow e^+(k_3) e^-(k_4). \quad (11)$$

The transition amplitude is a sum of photon- and Z- penguin diagrams (Fig. 1) and box diagrams (Fig. 2). There are two types of penguin diagrams in each case: those where the photon or Z is in the t-channel and those where it is in the s-channel (see Fig. 1). There is a relative minus sign between those diagrams due to Fermi statistics. The

contribution to the amplitude from the photon penguins has two form factors, $F_\gamma^{e\mu}$ and $G_\gamma^{e\mu}$ [7]:

$$i\mathcal{T}_\gamma = i\frac{\alpha_w^2 \sin^2 \theta_w}{2M_W^2} \left\{ \left[\bar{v}_\mu(k_1) \left(F_\gamma^{e\mu} \left(\gamma^\rho - \frac{q^\rho \not{q}}{q^2} \right) P_L - iG_\gamma^{e\mu} \frac{\sigma_{\rho\sigma} q^\sigma}{q^2} (m_e P_R + m_\mu P_L) \right) u_e(k_2) \right] \times [\bar{u}_e(k_4) \gamma_\rho v_e(k_3)] \right. \\ \left. - \left[v_e(k_3) \leftrightarrow u_e(k_2), \quad q \rightarrow q' \right] \right\}, \quad (q = k_1 + k_2, \quad q' = k_1 - k_3). \quad (12)$$

where $\alpha_w = g^2/(4\pi)$, $P_{R/L} = (1 \pm \gamma_5)/2$ are the chiral projectors, and $\sigma_{\rho\sigma} = (i/2)[\gamma_\rho, \gamma_\sigma]$. The term $q^\rho \not{q}$ vanishes when contracted to the vector current of the e^+e^- pair. Similarly, the Z penguins contain one form factor $F_Z^{e\mu}$:

$$i\mathcal{T}_Z = i\frac{\alpha_w^2}{4M_W^2} \left\{ F_Z^{e\mu} \left[\bar{v}_\mu(k_1) \gamma^\rho P_L u_e(k_2) \right] \times [\bar{u}_e(k_4) \gamma_\rho ((1 - 2\sin^2 \theta_w) P_L - 2\sin^2 \theta_w P_R) v_e(k_3)] \right. \\ \left. - \left[v_e(k_3) \leftrightarrow u_e(k_2) \right] \right\}, \quad (13)$$

and the box diagrams also one form factor, $F_B^{e\mu ee}$:

$$i\mathcal{T}_{\text{Box}} = i\frac{\alpha_w^2}{4M_W^2} F_B^{e\mu ee} \left[\bar{v}_\mu(k_1) \gamma^\rho P_L u_e(k_2) \right] \times [\bar{u}_e(k_4) \gamma_\rho P_L v_e(k_3)]. \quad (14)$$

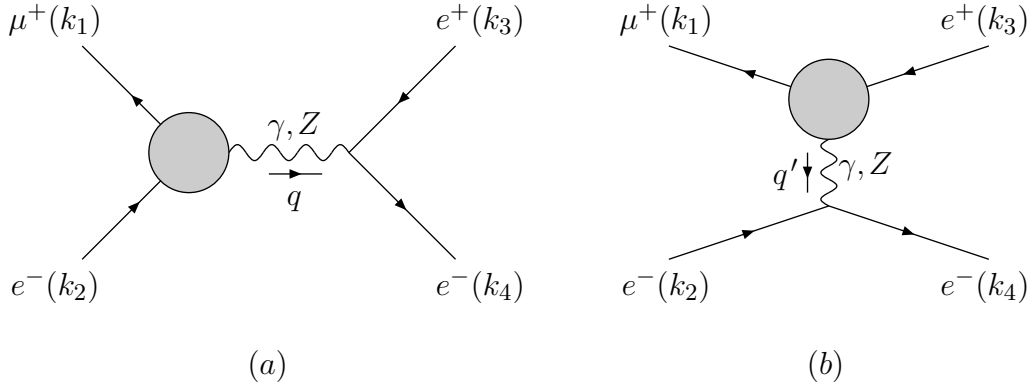


FIG. 1: The one-loop penguin diagrams for $\mu^+(k_1)e^-(k_2) \rightarrow e^+(k_3)e^-(k_4)$: (a) s-channel penguin and (b) t-channel penguin. The blob represents the loop involving W, G bosons and neutrinos. The diagram (b), *i.e.* t-channel, corresponds to the contributions in the last lines of Eqs. (12) and (13).

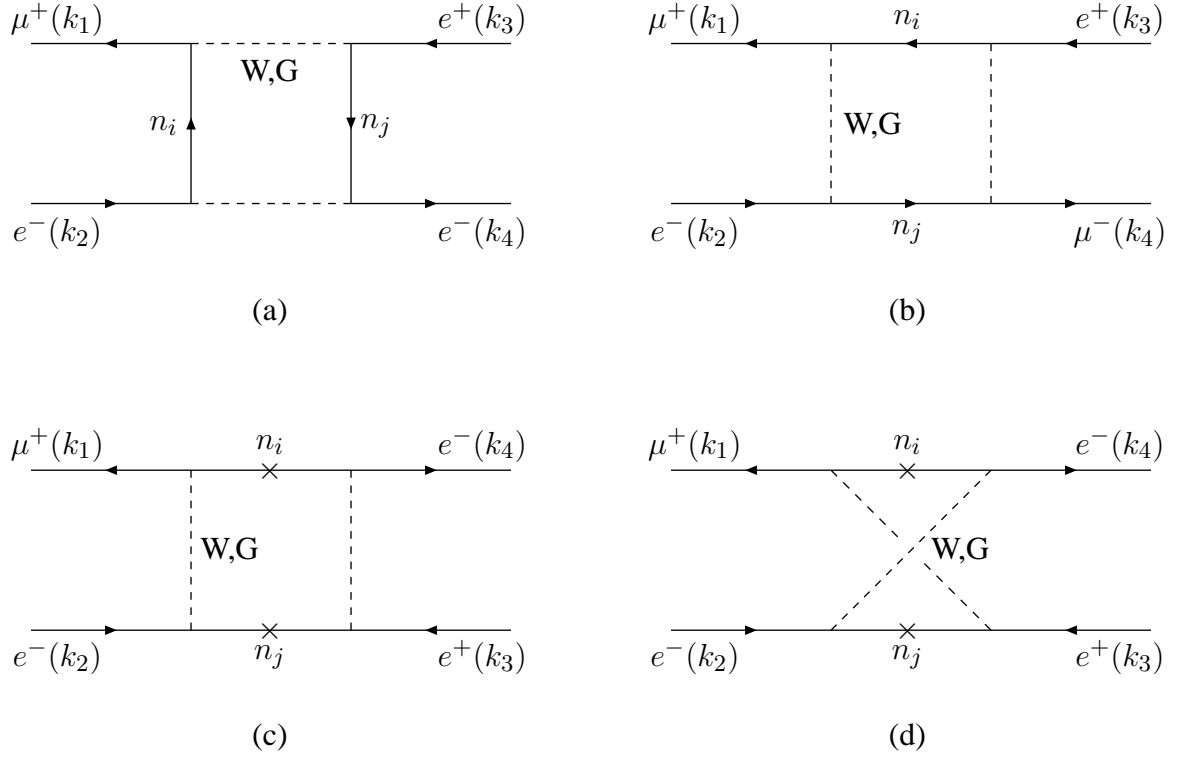


FIG. 2: The box diagrams for $\mu^+(k_1)e^-(k_2) \rightarrow e^+(k_3)e^-(k_4)$. The diagrams (b) and (d) are obtained from (a) and (c), respectively, by the exchange $e^-(k_2) \leftrightarrow e^+(k_3)$ and by the corresponding change in the flow of time.

The form factors $F_\gamma^{e\mu}$, $G_\gamma^{e\mu}$, $F_Z^{e\mu}$ and $F_B^{e\mu ee}$ are

$$F_\gamma^{e\mu} = \sum_{i=1}^{N_L+N_H} B_{ei}^* B_{\mu i} F_\gamma(x_i) \approx \sum_{I>N_L} B_{eI}^* B_{\mu I} F_\gamma(x_I), \quad (15)$$

$$G_\gamma^{e\mu} = \sum_{i=1}^{N_L+N_H} B_{ei}^* B_{\mu i} G_\gamma(x_i) \approx \sum_{I>N_L} B_{eI}^* B_{\mu I} G_\gamma(x_I), \quad (16)$$

$$F_Z^{e\mu} = \sum_{i,j=1}^{N_L+N_H} B_{ei}^* B_{\mu j} \left[\delta_{ij} F_Z(x_i) + C_{ij} H_Z(x_i, x_j) + C_{ij}^* G_Z(x_i, x_j) \right] \quad (17)$$

$$\approx \sum_{I>N_L} B_{eI}^* B_{\mu I} F_Z(x_I) + \sum_{I,J>N_L} B_{eI}^* B_{\mu J} [C_{IJ} H_Z(x_I, x_J) + C_{IJ}^* (G_Z(x_I, x_J) - G_Z(x_I, 0) - G_Z(0, x_J))] + 2 \sum_{I>N_L} B_{eI}^* B_{\mu I} G_Z(x_I, 0), \quad (18)$$

$$F_B^{e\mu ee} = \sum_{i,j=1}^{N_L+N_H} \left[2|B_{ei}|^2 B_{ej}^* B_{\mu j} F_{\text{Box}}(x_i, x_j) - (B_{ei}^*)^2 B_{ej} B_{\mu j} \lambda_j \lambda_i^* G_{\text{Box}}(x_i, x_j) \right] \quad (19)$$

$$\approx 2 \sum_{I,J>N_L} |B_{eI}|^2 B_{eJ}^* B_{\mu J} [F_{\text{Box}}(x_I, x_J) + F_{\text{Box}}(0, 0) - F_{\text{Box}}(x_I, 0) - F_{\text{Box}}(0, x_J)] - \sum_{I,J>N_L} (B_{eI}^*)^2 B_{eJ} B_{\mu J} \lambda_J \lambda_I^* G_{\text{Box}}(x_I, x_J) + 2 \sum_{J>N_L} B_{eJ}^* B_{\mu J} (F_{\text{Box}}(0, x_J) - F_{\text{Box}}(0, 0)), \quad (20)$$

where $x_i = m_i^2/M_W^2$ (m_i is the mass of the Majorana neutrino of type i inside the loop), and the functions $F_\gamma(x)$, $G_\gamma(x)$, $F_Z(x)$, $H_Z(x, y)$, $G_Z(x, y)$, $F_{\text{Box}}(x, y)$ and $G_{\text{Box}}(x, y)$ appear from the loop integrals [7], in the approximation where external masses and momenta are neglected. The explicit expressions of these functions are given in Ref. [16]. F_{Box} corresponds to the diagrams of Figs. 2(a) and (b), and G_{Box} to those of Figs. 2(c) and (d) which exist only

for Majorana neutrinos. Eqs. (15)-(19) involve summation over all 2-component neutrinos, where N_L is the number of standard (light) ones and N_H the number of extra (heavy) ones ($= N_L, 2N_L$ in Models I, II, respectively). All these expressions are identical to those obtained in Ref. [7] for neutrinoless lepton decays, except for the sign in front of the term proportional to $G_{\text{Box}}(x_i, x_j)$ – for details on the latter point, cf. Ref. [16]. Furthermore, in Eqs. (15)-(20) the expressions in a modified form are included which involve only the light-to-heavy mixing elements $B_{\ell I}$ ($\ell \leq N_L; I > N_L$); they are obtained by taking into account the unitarity of the U matrix, and the fact that the light neutrino masses are $m_\ell \ll M_W$.

The parameters λ_i are the creation phase factors[20] of the Majorana neutrinos n_i and n_j , respectively ($n_j^c = \lambda_j^* n_j$), which appear in the matrix Λ of Eq. (4). In the case of no CP violation and real mass matrix \mathcal{M} , we can choose the unitary matrix U as a real orthogonal matrix which diagonalizes the symmetric and real matrix \mathcal{M} ; then some of the λ_j 's are +1 and others are -1 [16]. Nonetheless we can choose all $\lambda_j = +1$, but then in general the unitary matrix U will not be real.

The total amplitude for $\mu^+ e^- \rightarrow e^+ e^-$ is then the sum of (12), (13) and (14).

IV. THE DECAY OF MUONIUM INTO $e^- e^+$

The calculation of the decay width of muonium M into $e^- e^+$ is determined by the LFV transition $\mu^+ e^- \rightarrow e^+ e^-$ at low momentum and by the muonium bound state wavefunction. The formula for the decay width of muonium M into a final state f is analogous to the expression for positronium decay:

$$d\Gamma(M \rightarrow f) = \frac{|\psi(0)|^2}{4\mu M} \frac{|\langle f | \mathcal{T} | \mu, e \rangle|^2}{|\langle f | \mathcal{T} | \mu, e \rangle|^2} dLips. \quad (21)$$

Here μ and M are the reduced mass and total mass of the bound state, respectively; $\psi(0)$ is the spatial wavefunction of the bound state at $\mathbf{x} = 0$; the bar over the matrix element means average over the initial spin components; and $dLips$ is the usual *Lorentz invariant phase space* of the final state, $dLips = \delta^4(p_f - p_i) d^3p_3 d^4p_4 / (16\pi^2 E_3 E_4)$.

The width can also be expressed in terms of the cross section of the constituents at low momentum, $\sigma(\mu^+ e^- \rightarrow f)$, since the latter involves the same transition element and phase space integral:

$$\Gamma(M \rightarrow f) = |\psi(0)|^2 \frac{\mathcal{S}_{12}}{2\mu M} \sigma(\mu^+ e^- \rightarrow f). \quad (22)$$

Here $\mathcal{S}_{12} \equiv 2 E_{CM} p_{CM}$ is the flux factor. At low momenta, the factor $\mathcal{S}_{12}/2\mu M$ reduces to the relative velocity between the constituents, v_{rel} . Since muonium is a rather nonrelativistic Coulomb bound state, the wavefunction is calculable:

$$|\psi(0)|^2 = \frac{\alpha_{em}^3 \mu^3}{\pi} = \frac{\alpha_{em}^3}{\pi} \frac{m_e^3}{(1 + m_e/m_\mu)^3} \quad (23)$$

and is independent of the final state f into which the constituents disintegrate. On the other hand, the disintegration process itself is totally contained in the cross section $\sigma(\mu^+ e^- \rightarrow f)$. Using the two previous expressions, the decay $M \rightarrow e^- e^+$ results in:

$$\Gamma(M \rightarrow e^- e^+) = \left[\frac{\alpha_{em}^3}{\pi} \frac{m_e^3}{(1 + m_e/m_\mu)^3} \right] v_{\text{rel}} \sigma(e^- \mu^+ \rightarrow e^- e^+) \Big|_{v_{\text{rel}} \rightarrow 0}. \quad (24)$$

Therefore, the calculation of this decay rate reduces to the calculation of the scattering cross section $\sigma(e^- \mu^+ \rightarrow e^- e^+)$ at low (nonrelativistic) momentum. We remark that the factor v_{rel} in Eq. (24) will cancel the corresponding factor $1/v_{\text{rel}}$ contained in the cross section. Now, let us find the decay rate within Models I and II described in the previous section.

Although our expressions for the amplitude and form factors are the same as those of Ref. [7] for lepton decays, the matrix element for muonium decay becomes a different combination of form factors, because the kinematic regime in muonium decay is quite different than that in free lepton decay: in muonium, we should take the initial 3-momenta as non-relativistic (or vanishing, since the amplitudes are smooth functions of momenta). The result for the total

amplitude squared, summed over final spins and averaged over initial spins, is then:

$$\begin{aligned} \overline{|\mathcal{T}_{\text{total}}|^2} = \frac{\alpha_w^4}{16M_W^4} \Big\{ & (m_e m_\mu^3 + 2m_e^2 m_\mu^2 + m_e^3 m_\mu) |2F_Z^{e\mu} + F_B^{e\mu ee}|^2 \\ & + 4\sin^2 \theta_w (2m_e m_\mu^3 + 3m_e^2 m_\mu^2 + 3m_e^3 m_\mu) \operatorname{Re} [(2F_Z^{e\mu} + F_B^{e\mu ee})(F_\gamma^{e\mu} - F_Z^{e\mu})^*] \\ & + 12\sin^2 \theta_w (m_e m_\mu^3 + 2m_e^2 m_\mu^2 + m_e^3 m_\mu) \operatorname{Re} [(2F_Z^{e\mu} + F_B^{e\mu ee})G_\gamma^{e\mu}] \\ & + 4\sin^4 \theta_w (7m_e m_\mu^3 + 12m_e^2 m_\mu^2 + 9m_e^3 m_\mu) |F_\gamma^{e\mu} - F_Z^{e\mu}|^2 \\ & + 4\sin^4 \theta_w (-2m_\mu^4 + 12m_e m_\mu^3 + 36m_e^2 m_\mu^2 + 18m_e^3 m_\mu) \operatorname{Re} [(F_\gamma^{e\mu} - F_Z^{e\mu})G_\gamma^{e\mu}] \\ & + 4\sin^4 \theta_w \left(\frac{m_\mu^5}{m_e} + 2m_\mu^4 + 8m_e m_\mu^3 + 24m_e^2 m_\mu^2 + 9m_e^3 m_\mu \right) |G_\gamma^{e\mu}|^2 \Big\}. \end{aligned} \quad (25)$$

From this expression and Eq. (24) one obtains the muonium decay rate, after integration over phase space. Since the amplitude is independent of the kinematics in the non-relativistic limit, the integration is simply $\int dLips = (1/8\pi)\sqrt{1 - 4m_e^2/(m_\mu + m_e)^2}$, and we have

$$\Gamma(M \rightarrow e^+ e^-) = \frac{\alpha_{em}^3 m_e m_\mu}{32\pi^2} \frac{m_\mu^3}{(m_\mu + m_e)^3} \sqrt{\left[1 - 4\frac{m_e^2}{(m_\mu + m_e)^2}\right]} \overline{|\mathcal{T}_{\text{total}}|^2} \quad (26)$$

$$= \frac{\alpha_{em}^3 m_e m_\mu}{32\pi^2} \frac{m_\mu}{m_\mu} \left[1 - 3\frac{m_e}{m_\mu} + \mathcal{O}\left(\frac{m_e^2}{m_\mu^2}\right)\right] \overline{|\mathcal{T}_{\text{total}}|^2}, \quad (27)$$

where $\overline{|\mathcal{T}_{\text{total}}|^2}$ is given in Eq. (25). Now, comparing Eq. (26) with the tree-level expression for the muon width $\Gamma(\mu \rightarrow all)^{(0)} = G_F^2 m_\mu^5 / (192\pi^3)$, which is comparable to the *muonium* width, we obtain the branching ratio:

$$\begin{aligned} Br(M \rightarrow e^+ e^-) &\equiv \frac{\Gamma(M \rightarrow e^+ e^-)}{\Gamma(\mu \rightarrow all)^{(0)}} \\ &= \frac{3}{\pi} \alpha_{em}^5 \left(\frac{m_e}{m_\mu}\right) \frac{m_\mu^3}{(m_\mu + m_e)^3} \sqrt{\left[1 - 4\frac{m_e^2}{(m_\mu + m_e)^2}\right]} \frac{1}{\sin^4 \theta_w} B_{\text{red.}} \approx 1.77 \cdot 10^{-12} B_{\text{red.}}, \end{aligned} \quad (28)$$

where we defined a reduced branching ratio $B_{\text{red.}}$:

$$B_{\text{red.}} = \frac{4}{\alpha_W^4} \frac{M_W^4 m_e}{m_\mu^5} \overline{|\mathcal{T}_{\text{total}}|^2}, \quad (29)$$

with $\overline{|\mathcal{T}_{\text{total}}|^2}$ given by (25). Provided the neutrino masses are below a few TeV, a rather good approximation for $B_{\text{red.}}$ is obtained by expanding Eq. (25) to second order in (m_e/m_μ) :

$$\begin{aligned} B_{\text{red.}} &= \left\{ \sin^4 \theta_w |G_\gamma|^2 - 2\left(\frac{m_e}{m_\mu}\right) \sin^4 \theta_w \operatorname{Re} [(F_\gamma - F_Z)G_\gamma^* - |G_\gamma|^2] \right. \\ &\quad + \frac{1}{4} \left(\frac{m_e}{m_\mu}\right)^2 \left[|F_B + 2F_Z + 4\sin^2 \theta_w (F_\gamma - F_Z) + 6\sin^2 \theta_w G_\gamma|^2 \right. \\ &\quad \left. \left. + 4\sin^4 \theta_w (3|F_\gamma|^2 - |G_\gamma|^2 + 3|F_Z|^2 - 6\operatorname{Re}(F_Z F_\gamma^*)) \right] + \mathcal{O}\left(\frac{m_e^3}{m_\mu^3}\right) \right\}. \end{aligned} \quad (30)$$

For simplicity of notation we have omitted the superscripts $e\mu$ and $e\mu ee$ in the form factors. We see that the box diagrams (*i.e.*, the form factors F_{Box}) have in general only a small effect on this process. This contrasts with muonium to antimuonium conversion, where the box diagrams are the only contribution [16]. This is a bit disappointing, since it is only in the box diagrams where the true Majorana character of neutrinos appear, as seen in Figs. 2(c) and (d). The rest of the diagrams are sensitive to the neutrino masses and mixings, irrespective of their Dirac or Majorana character. In the next section we will see, however, that the free $\mu^+ e^-$ scattering at high energy depends on a different combination of form factors, where the box diagrams do enter. In this sense, $\mu^+ e^-$ scattering at high energy is complementary to muonium decay, when testing this LFV process.

In order to obtain numerical results, the parameter space of the models must first be reasonably narrowed down. First the parameters appearing in the Dirac matrix m_D , Eq. (2), are chosen in such a way as to fulfill, at fixed

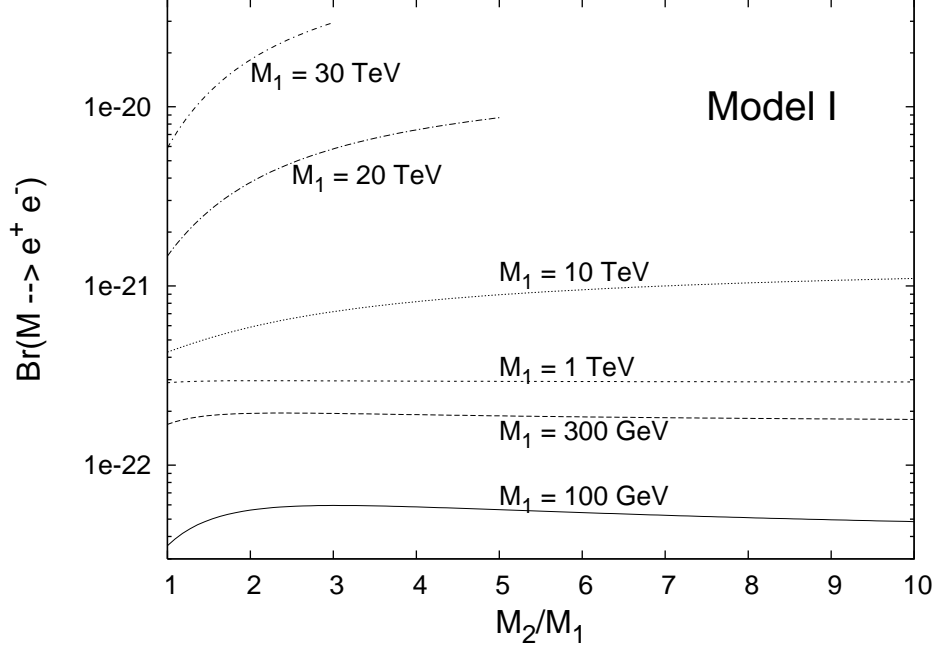


FIG. 3: The branching ratio $\Gamma(M \rightarrow e^+e^-)/\Gamma(\mu \rightarrow all)^{(0)}$, Eq. (28) in Model I, for the (approximately) optimal choice [cf. Eq. (31)] for the Dirac mass parameters, as a function of the neutrino mass ratio $M_2/M_1 (\geq 1)$, and for different $M_1 = 100$ GeV, 300 GeV, 1 TeV, 10 TeV, 20 TeV and 30 TeV, as indicated. The last two curves are shown only up to $M_2/M_1 \approx 5$ and 3, respectively, due to the perturbative unitarity bound [7].

Majorana masses M_1 and M_2 , all the experimental requirements, and at the same time to approach maximal squared amplitudes (e.g. $|G_\gamma|^2$ etc.) appearing in the decay width of Eqs. (28) and (29) (see Refs. [15, 16] for details), in order to find the most favorable case to observe such rare processes. This optimal condition fixes the model parameters as follows:

$$\begin{aligned} \text{Model I : } a &= c = \frac{M_1 s_L}{\sqrt{1 + M_1/M_2}}, \\ b &= -d = a \sqrt{M_2/M_1}, \quad \delta_1 = \delta_2 = \pi/2, \end{aligned} \quad (31)$$

$$\begin{aligned} \text{Model II : } a &= \frac{M_2 s_L^{\nu_e}}{\sqrt{(M_2/M_1)^2 + (s_L^{\nu_\mu}/s_L^{\nu_e})^2}}, \\ b &= c = a \times (s_L^{\nu_\mu}/s_L^{\nu_e}), \quad d = a \times (s_L^{\nu_\mu}/s_L^{\nu_e})^2, \quad \delta_1 = \delta_2 = 0. \end{aligned} \quad (32)$$

Here, $(s_L^{\nu_\ell})^2 \equiv \sum_h |B_{\ell h}|^2$ ($N_L < h \leq N_L + N_H$; $\ell = e, \mu$) are the light-to-heavy mixings, and s_L in (31) means the common value $s_L^{\nu_e} = s_L^{\nu_\mu}$. The squares $|A_p|^2$ of the penguin diagrams A_p , for the parameter choices (31) and (32), are approximately proportional to $(s_L^{\nu_\mu})^2 (s_L^{\nu_e})^2$, as shown in Appendix of Ref. [15] on the basis of unitarity of matrix U . The quantity $Br(M \rightarrow e^+e^-)$ is dominated by the penguin diagrams, as seen earlier in this Section. Further, the other quantities considered later on in this work (cross sections for $e^- \mu^+ \rightarrow e^- e^+$ and for $e^- \mu^+ \rightarrow WW$), are also approximately proportional to $(s_L^{\nu_\mu})^2 (s_L^{\nu_e})^2$.¹ While each of the two mixings separately is restricted by inequalities [24]

$$(s_L^{\nu_e})^2 \leq 0.005, \quad (s_L^{\nu_\mu})^2 \leq 0.002, \quad (33)$$

there is a strong restriction on the product of the two mixings: $s_L^{\nu_e} s_L^{\nu_\mu} < 0.00012$. The latter restriction is obtained in the two models, with parameter choice (31) and (32), when the models are required to give predictions for the

¹ For the box diagrams there can be substantial deviations from such proportionality, especially when matrix U is not real.

branching ratio $Br(\mu^- \rightarrow e^- \gamma)$ which respect the experimental upper bound [25]:

$$Br(\mu^- \rightarrow e^- \gamma) < 1.2 \times 10^{-11} . \quad (34)$$

More specifically, the aforementioned upper bound for $s_L^{\nu_e} s_L^{\nu_\mu}$ is obtained from restriction (34) because

$$Br(\mu^- \rightarrow e^- \gamma) = \alpha_{em} \frac{3}{2\pi} |G_\gamma^{e\mu}|^2 , \quad (35)$$

and it can be shown that $|G_\gamma^{e\mu}|^2 \leq (1/4)(s_L^{\nu_\mu})^2 (s_L^{\nu_e})^2$, where approximate equality is obtained when the parameters are chosen according to Eqs. (31) and (32) in models I and II, respectively. We will choose $s_L^{\nu_e} = s_L^{\nu_\mu} \equiv s_L$. Therefore, we will take in (31) and (32) the saturated values

$$(s_L)^2 = (s_L^{\nu_e})^2 = (s_L^{\nu_\mu})^2 = 1.2 \times 10^{-4} . \quad (36)$$

For simplicity, we restricted Model II to cases with no CP violation ($\delta_1 = \delta_2 = 0$). The heavy neutrino masses M_1 and M_2 are restricted to be above 100 GeV, and we take the convention $M_1 < M_2$. There is also an upper bound for M_1 and M_2 in the form $M_h^2 \sum_\ell |B_{\ell h}|^2 < 2M_W^2/\alpha_W$, with $\ell = e, \mu$ [7], due to the breakdown of perturbative expansion to one loop above this bound. In Model I, this bound, in conjunction with restrictions (36), translates into a restriction which is approximately of the form $M_1 \cdot M_2 \lesssim (50 \text{ TeV})^2$, while for Model II the bound allows any value of M_2 ($\geq M_1$) as long as $M_1 \lesssim 60 \text{ TeV}$.

The numerical results for the branching ratio $Br(M \rightarrow e^+ e^-)$ defined in Eq. (28) are given in Fig. 3 and Fig. 4, for Model I and Model II, respectively. We see that the branching ratios are extremely small, mainly because of the factor

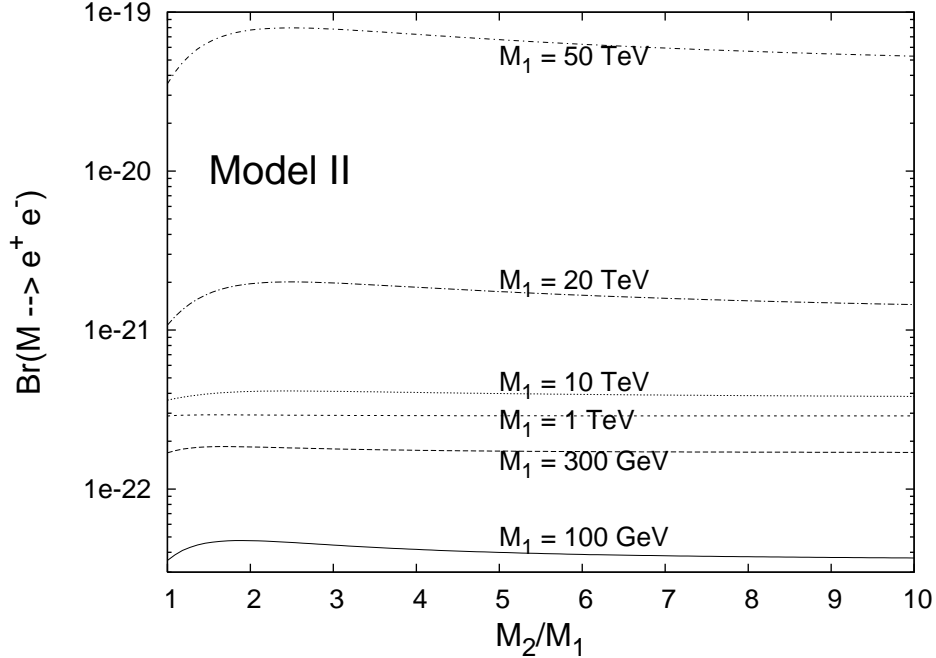


FIG. 4: Same as in Fig. 3, but this time for Model II, for the (approximately) optimal choice (32) for the Dirac mass parameters. The curves, including the ones with $M_1 = 20$ and 50 TeV, are in this model allowed by the PUB.

$\sim 10^{-12}$ appearing in Eq. (28). Two major sources for this suppression are a factor α_{em}^3 coming from the muonium wavefunction and a factor α_{em}^2 from the one-loop character of the squared amplitude. Another source of suppression are the small upper bounds (36) on the mixing-parameters. From Figs. 3 and 4 we see that the branching ratios in both models cannot surpass 10^{-19} . These values are so small that they seem out of the reach of experiments in the foreseeable future.

V. $\mu^+ e^- \rightarrow e^+ e^-$ COLLISIONS AT HIGH ENERGY

In addition to muonium decay, one can study the free scattering process $\mu^+ e^- \rightarrow e^+ e^-$ at higher energies. The cross section in the center-of-mass system (CMS) for this process at energies well above the muon mass follows from

the same amplitudes (12), (13) and (14), but the form factors enter in a quite different combination because of the different kinematic regime. Indeed, for CM energies \sqrt{s} in the range $m_\mu \ll \sqrt{s} \ll M_W$, the cross section is:

$$\begin{aligned} \sigma(e^- \mu^+ \rightarrow e^- e^+; s) \\ = \frac{1}{12\pi} \left(\frac{\alpha_w^2}{4M_W^2} \right)^2 s \left[|(1 - 2\sin^2 \theta_w) F_Z^{e\mu} + 2\sin^2 \theta_w F_\gamma^{e\mu} + \frac{1}{2} F_{\text{Box}}^{e\mu ee}|^2 + 4\sin^4 \theta_w |F_\gamma^{e\mu} - F_Z^{e\mu}|^2 \right]. \end{aligned} \quad (37)$$

The numerical results, for Models I and II at various chosen heavy neutrino masses M_1 and M_2 , are given in Figs. 5 (a) and (b), respectively. The elements of the Dirac mass m_D are again chosen in the optimized forms (31) and (32),

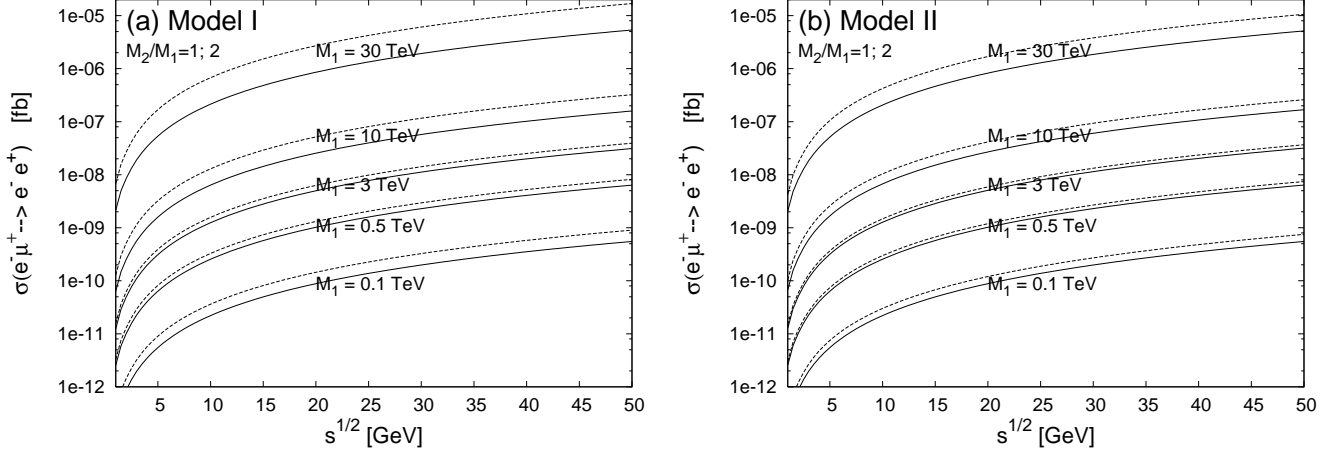


FIG. 5: The cross section for the LFV scattering process $e^- \mu^+ \rightarrow e^- e^+$ as a function of CMS energy \sqrt{s} in (a) Model I, and (b) Model II. In all cases, each pair of curves corresponds to a given value of M_1 and to the values of $M_2/M_1 = 1$ (solid line) and $M_2/M_1 = 2$ (dotted line).

respectively, and the mixing parameters have the upper bound values (36).

As shown in Figs. 5, the cross sections in both models are of the same order of magnitude, the ones in Model I being slightly larger than the corresponding ones in Model II. These cross sections are however very small. If one expects integrated luminosities not much larger than a few fb^{-1} at an hypothetical muon collider, then an experimental test of this process is not likely to be viable.

VI. UNSUPPRESSED SCATTERING CHANNEL $e\mu \rightarrow WW$

To complement our analysis of the LFV scattering process $\mu^+ e^- \rightarrow e^+ e^-$, we consider the case of open W production.

When we consider $e^- \mu^+$ scattering at CMS energies above the $W^+ W^-$ production threshold, the unsuppressed tree-level channel $e^- \mu^+ \rightarrow W^- W^+$ opens up. This process is mediated by a neutrino exchange, as depicted in Fig. 6. Here we will limit ourselves to estimate the cross section of the process. However, it is understood that the experimental observation of this process is hindered not just by the smallness of the cross section, but also by the rejection of background events that contain neutrinos in the final state.

The amplitude \mathcal{T} for $\mu^+ e^- \rightarrow W^+ W^-$ is

$$\mathcal{T} = -i \frac{g_w^2}{2} B_{\mu j} B_{ej}^* \frac{1}{[(p_1 - k_1)^2 - m_j^2 + i\varepsilon]} [\bar{v}(k_1) \not{\epsilon}(p_1)^* (\not{p}_1 - \not{k}_1) \not{\epsilon}(p_2)^* P_L u(k_2)] , \quad (38)$$

where ϵ is the W -polarization vector. Consequently the total cross section for the process is:

$$\sigma(e^- \mu^+ \rightarrow WW; s) = \frac{1}{64\pi} \left(\frac{g_w^2}{2} \right)^2 \frac{1}{s^2} \sum_{i,j=1}^{N_L+N_H} (B_{ej}^* B_{\mu j} B_{ei} B_{\mu i}^*) A_{ij} \quad (39)$$

$$= \frac{1}{64\pi} \left(\frac{g_w^2}{2} \right)^2 \frac{1}{s^2} \sum_{I,J>N_L} (B_{eJ}^* B_{\mu J} B_{eI} B_{\mu I}^*) (A_{IJ} + A_{\ell\ell} - A_{\ell J} - A_{I\ell}) , \quad (40)$$

where the explicit expressions of the coefficients $A_{ij}(m_i^2, m_j^2, M_W^2, s)$ are written in Appendix. To go from Eq. (39) to Eq. (40) we used unitarity of the mixing matrix (the index ℓ in A_{ij} denotes a light neutrino state, whose mass we can neglect). The Dirac mass matrix m_D for models I and II is again chosen in the forms (31) and (32), respectively, and the mixing-parameter values are those of Eq. (36).

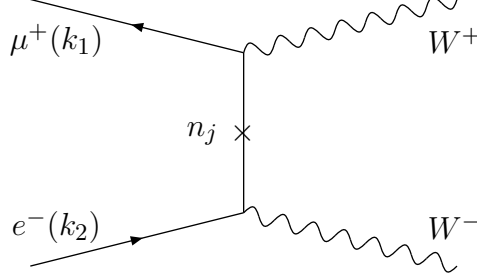


FIG. 6: The tree-level process $e^- \mu^+ \rightarrow W^- W^+$ via exchange of a Majorana neutrino.

The numerical results for Models I and II, and various chosen heavy Majorana neutrino masses M_1 and M_2 , are given in Figs. 7 (a) and (b), respectively.

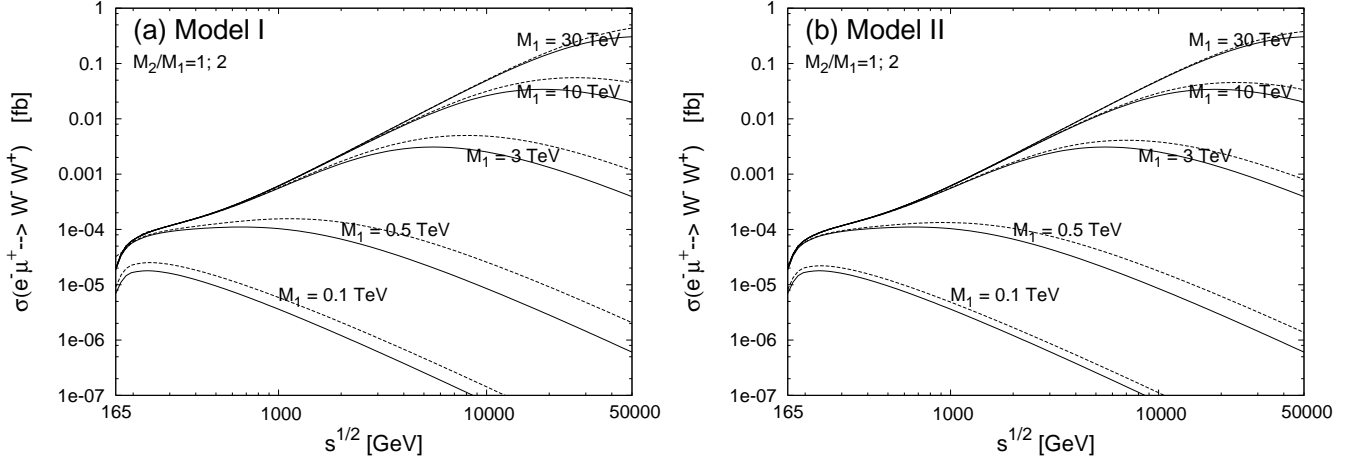


FIG. 7: The cross section for the LFV scattering process $e^- \mu^+ \rightarrow W^- W^+$ as a function of CMS energy \sqrt{s} in (a) Model I, and (b) Model II. Each pair of curves corresponds to the indicated value of M_1 , and $M_2/M_1 = 1$ (solid line) or 2 (dotted line).

We can see that the open $W^+ W^-$ production cross section at $\sqrt{s} \sim 200$ GeV is between 10^{-5} and 10^{-4} fb, which is in general several orders of magnitude larger than the cross section for $e^+ e^-$ production for CMS energies below the $W^+ W^-$ threshold,² but it is still very small. As a reference, the point cross section $\sigma(e^+ e^- \rightarrow \gamma^* \rightarrow \mu^+ \mu^-)$ at $\sqrt{s} = 200$ GeV is close to 2 pb, which is 7 orders of magnitude larger.

VII. CONCLUSIONS

In the present work we have studied the possibility to observe lepton flavor violating effects in $\mu^+ e^-$ annihilation processes induced by heavy neutrino scenarios. We use two scenarios: one that is a plain seesaw model that violates both lepton flavor and lepton number (Model I) and another that has a richer spectrum of neutral fermions and violates lepton flavor while conserving lepton number (Model II). In a previous work[16] we have studied these scenarios in the case of muonium to antimuonium conversion, which is box-diagram dominated and reflects the underlying process $\mu^+ e^- \rightarrow \mu^- e^+$. Here we were interested in the process $\mu^+ e^- \rightarrow e^+ e^-$ which is in general penguin-diagram dominated.

² If M_1 and M_2 are very large (> 10 TeV), the two cross sections at $\sqrt{s} \sim 200$ GeV are comparable, $\sim 10^{-4}$ - 10^{-5} fb.

We studied this process both at low and high center-of-momentum energies. At low (non-relativistic) energy, this corresponds to the muonium decay $M \rightarrow e^+e^-$. In both scenarios the branching ratios are exceedingly small (less than 10^{-19}), basically because, besides the smallness imposed by a LFV process, there is an extra factor α_{em}^3 arising from the muonium wavefunction. To avoid this suppression, the alternative is to consider the collision μ^+e^- at higher energies. We find the cross section for $\mu^+e^- \rightarrow e^+e^-$ to rise with energy, but reaching at most 10^{-5} fb at $\sqrt{s} \sim 50$ GeV. If one expects integrated luminosities not much larger than a few fb^{-1} at a future muon collider, then this process is not likely to be observed. Finally, we have pushed to very high energies, namely above the W^+W^- production threshold. Only in that case we find that the two scenarios, Model I and Model II, would induce cross sections for $\mu^+e^- \rightarrow W^+W^-$ up to the order of 10^{-1} fb or 1 fb. This process, however, has the additional experimental difficulty that it needs to be distinguished from the standard background where two neutrinos are present in the final state.

Acknowledgments

C.D. acknowledges support from Fondecyt (Chile) research grant No. 1030254 and G.C. from Fondecyt grants No. 1050512 and No. 7010094. The work of C.S.K. was supported in part by the CHEP-SRC Program and by the Korea Research Foundation Grant funded by the Korean Government (MOEHRD) No. KRF-2005-070-C00030. The work of J.D.K was supported by the Korea Research Foundation Grant (2001-042-D00022).

-
- [1] B. T. Cleveland *et al.* [Homestake Coll.], *Astrophys. J.* **496**, 505 (1998); Y. Fukuda *et al.* [Kamiokande Coll.], *Phys. Rev. Lett.* **77**, 1683 (1996); J. N. Abdurashitov *et al.* [SAGE Coll.], *J. Exp. Theor. Phys.* **95**, 181 (2002); W. Hampel *et al.* [GALLEX Coll.], *Phys. Lett. B* **447**, 127 (1999); M. Altmann *et al.* [GNO Coll.], *Phys. Lett. B* **616**, 174 (2005); S. N. Ahmed *et al.* [SNO Coll.], *Phys. Rev. Lett.* **92**, 181301 (2004); T. Araki *et al.* [KamLAND Coll.], *Phys. Rev. Lett.* **94**, 081801 (2005); Y. Ashie *et al.* [Super-Kamiokande Coll.], *Phys. Rev. Lett.* **93**, 101801 (2004); For a review, see e.g. G. L. Fogli, E. Lisi, A. Marrone, A. Palazzo and A. M. Rotunno, *40th Rencontres de Moriond on Electroweak Interactions and Unified Theories*, La Thuile, Aosta Valley, Italy, 5-12 Mar 2005, arXiv:hep-ph/0506307.
 - [2] J. Schechter and J. W. F. Valle, *Phys. Rev. D* **22**, 2227 (1980).
 - [3] T. Yanagida, *Proceedings of the Workshop on Unified Theory and Baryon Number of the Universe*, eds. O. Swada and A. Sugamoto (KEK, 1979) p.95; M. Gell-Mann, P. Ramond and R. Slansky, *Supergravity*, eds. P. van Nieuwenhuizen and D. Friedman (North-Holland, Amsterdam, 1979) p. 315; R. N. Mohapatra and G. Senjanović, *Phys. Rev. Lett.* **44**, 912 (1980).
 - [4] E. Witten, *Nucl. Phys. B* **268**, 79 (1986); R. N. Mohapatra and J. W. Valle, *Phys. Rev. D* **34**, 1642 (1986); J. L. Hewett and T. G. Rizzo, *Phys. Rept.* **183** (1989) 193.
 - [5] D. Wyler and L. Wolfenstein, *Nucl. Phys. B* **218**, 205 (1983).
 - [6] B. W. Lee and R. E. Shrock, *Phys. Rev. D* **16**, 1444 (1977).
 - [7] A. Ilakovac and A. Pilaftsis, *Nucl. Phys. B* **437**, 491 (1995).
 - [8] J. G. Körner, A. Pilaftsis and K. Schilcher, *Phys. Rev. D* **47**, 1080 (1993).
 - [9] M. C. Gonzalez-Garcia and J. W. Valle, *Mod. Phys. Lett. A* **7**, 477 (1992).
 - [10] Y. Okada, K. i. Okumura and Y. Shimizu, *Phys. Rev. D* **58**, 051901 (1998); *ibid.* **61**, 094001 (2000).
 - [11] A. Kageyama, S. Kaneko, N. Shimoyama and M. Tanimoto, *Phys. Lett. B* **527**, 206 (2002); *ibid.* *Phys. Rev. D* **65**, 096010 (2002).
 - [12] B. Pontecorvo, *Sov. Phys. JETP* **6**, 429 (1957); G. Feinberg and S. Weinberg, *Phys. Rev.* **123**, 1439 (1961); A. Halprin, *Phys. Rev. Lett.* **48**, 1313 (1982); A. Halprin and A. Masiero, *Phys. Rev. D* **48**, R2987 (1993); P. Herczeg and R. N. Mohapatra, *Phys. Rev. Lett.* **69**, 2475 (1992);
 - [13] T. Huber *et al.*, *Phys. Rev. D* **41**, 2709 (1990); B. Matthias *et al.*, *Phys. Rev. Lett.* **66**, 2716 (1991); R. Abela *et al.*, *Phys. Rev. Lett.* **77**, 1950 (1996); L. Willmann *et al.*, *Phys. Rev. Lett.* **82**, 49 (1999).
 - [14] A. Czarnecki, G. P. Lepage and W. J. Marciano, *Phys. Rev. D* **61**, 073001 (2000).
 - [15] G. Cvetič, C. Dib, C. S. Kim and J. D. Kim, *Phys. Rev. D* **66**, 034008 (2002)
 - [16] G. Cvetič, C. O. Dib, C. S. Kim and J. D. Kim, *Phys. Rev. D* **71**, 113013 (2005)
 - [17] G. C. Branco, M. N. Rebelo and J. W. F. Valle, *Phys. Lett. B* **225**, 385 (1989).
 - [18] M. C. Gonzalez-Garcia and J. W. Valle, *Phys. Lett. B* **216**, 360 (1989).
 - [19] B. Kayser, *Phys. Rev. D* **30**, 1023 (1984).
 - [20] B. Kayser, F. Gibrat-Debu, and F. Perrier, *The Physics of Massive Neutrinos* (World Scientific, Singapore, 1989).
 - [21] A. Pilaftsis, *Z. Phys. C* **55**, 275 (1992)
 - [22] C. Itzykson and J.-B. Zuber, *Quantum Field Theory* (McGraw-Hill, New York, 1980).
 - [23] M. Jamin and M. E. Lautenbacher, *Comput. Phys. Commun.* **74**, 265 (1993).
 - [24] E. Nardi, E. Roulet and D. Tommasini, *Phys. Lett. B* **327**, 319 (1994); *ibid.* **344**, 225 (1995).
 - [25] W. M. Yao *et al.* [Particle Data Group], *J. Phys. G* **33**, 1 (2006).

APPENDIX A: FUNCTIONS A_{ij} FOR $e\mu \rightarrow WW$ SCATTERING

The coefficient functions $A_{ij}(m_i^2, m_j^2, M_W^2, s)$ appearing in the sum (39) are long expressions obtained by calculating a Trace that follows from squaring the amplitude (38). For this, we used the program Tracer [23]. When neglecting m_μ in comparison to M_W and \sqrt{s} , the result for $i \neq j$ is

$$\begin{aligned}
A_{ij} = & \frac{1}{[48(m_i - m_j)(m_i + m_j)M_W^4]} \left\{ (m_i - m_j)(m_i + m_j)s\mathcal{K} \right. \\
& \times [-6(m_i^4 + m_i^2m_j^2 + m_j^4) + 6(m_i^2 + m_j^2)M_W^2 - 24M_W^4 - (3(m_i^2 + m_j^2) - 20M_W^2)s + s^2] \\
& - 6[(m_i^2 - M_W^2)^2(m_i^4 + 4M_W^4) + (m_i^3 - 2m_iM_W^2)^2s]\mathcal{L}_i \\
& \left. + 6[(m_j^2 - M_W^2)^2(m_j^4 + 4M_W^4) + (m_j^3 - 2m_jM_W^2)^2s]\mathcal{L}_j \right\}, \tag{A1}
\end{aligned}$$

$$\begin{aligned}
A_{jj} = & \frac{1}{48M_W^4} \frac{s\mathcal{K}}{[(m_j^2 - M_W^2)^2 + m_j^2s]} \left[-24m_j^8 + 30m_j^6(2M_W^2 - s) + m_j^4(-96M_W^4 + 68M_W^2s - 5s^2) \right. \\
& \left. + M_W^4(-48M_W^4 + 20M_W^2s + s^2) + m_j^2(108M_W^6 - 94M_W^4s + 18M_W^2s^2 + s^3) \right] \\
& - \frac{1}{8M_W^4} \left[4m_j^6 + 4M_W^4(-2 * M_W^2 + s) + m_j^4(-6M_W^2 + 3s) + 2m_j^2(5M_W^4 - 4M_W^2s) \right] \mathcal{L}_j, \tag{A2}
\end{aligned}$$

where we used the short-hand notations

$$\mathcal{K} = \left[1 - \frac{4M_W^2}{s} \right]^{1/2}, \quad \mathcal{L}_k = \ln \left[\frac{(2m_k^2 - 2M_W^2 + s - s\mathcal{K})}{(2m_k^2 - 2M_W^2 + s + s\mathcal{K})} \right]. \tag{A3}$$